






# Magnetic nano-biocomposite $\text{CuFe}_2\text{O}_4$ @methylcellulose (MC) prepared as a new nano-photocatalyst for degradation of ciprofloxacin from aqueous solution

Alireza Nasiri<sup>1,2</sup>, Fatemeh Tamaddon<sup>3\*</sup>, Mohammad Hossein Mosslemin<sup>1</sup>, Majid Amiri Gharaghani<sup>4</sup>,  
Ali Asadipour<sup>2</sup>

<sup>1</sup>Department of Chemistry, Islamic Azad University, Yazd Branch, Yazd, Iran

<sup>2</sup>Environmental Health Engineering Research Center, Kerman University of Medical Sciences, Kerman, Iran

<sup>3</sup>Department of Chemistry, Yazd University, Yazd 89195-741, Iran

<sup>4</sup>Department of Environmental Health Engineering, Sirjan Faculty of Medical Science, Sirjan, Iran

## Abstract

**Background:** Antibiotics such as ciprofloxacin (CIP) are even more important in bacterial resistance, even at low concentrations. The aim of this research was to synthesize  $\text{CuFe}_2\text{O}_4$ @methylcellulose (MC) as a new nano-photocatalyst for degradation of CIP from aqueous solution.

**Methods:** The nano-photocatalyst ( $\text{CuFe}_2\text{O}_4$ @MC) was characterized by FESEM, energy dispersive spectroscopy (EDS), X-ray diffraction (XRD) and Fourier transform infrared (FTIR), thermogravimetric analysis (TGA), and vibrating sample magnetometer (VSM). Powder XRD and EDS analysis confirmed the formation of pure-phase spinel ferrites. After  $\text{CuFe}_2\text{O}_4$ @MC characterization, the effective parameters in removal efficiency of CIP such as reaction time, initial antibiotic concentration, pH, photocatalyst loading, and degradation kinetic were investigated and conditions were optimized. Then, CIP degradation experiments were conducted on the real sample in the optimal conditions. The removal of chemical oxygen demand (COD) was determined under optimum conditions.

**Results:** The structural characterization of the magnetic nanobiocomposite showed that it is in nanoscale, ferromagnetic property, and thermal stability. The optimal conditions were obtained at pH = 7, irradiation time (90 minutes), photocatalyst loading (0.2 g), and initial concentration of CIP (3 mg/L). The removal efficiency of CIP in the optimal conditions was obtained as 80.74% and 72.87% from the synthetic and real samples, respectively. The removal of COD was obtained as 68.26% in this process. The evaluation of kinetic linear models showed that the photocatalytic degradation process was fitted by pseudo-first order kinetic model and Langmuir-Hinshelwood.  $\text{CuFe}_2\text{O}_4$ @MC photocatalyst had a good stability and reusability for the fourth runs.

**Conclusion:** The photocatalytic degradation of CIP from aqueous media with  $\text{CuFe}_2\text{O}_4$ @MC photocatalyst has a high efficiency, which can be used in the treatment of pharmaceutical wastewaters.

**Keywords:** Spinel, Ciprofloxacin, Methylcellulose, Wastewater

**Citation:** Nasiri A, Tamaddon F, Mosslemin MH, Amiri Gharaghani M, Asadipour A. Magnetic nano-biocomposite  $\text{CuFe}_2\text{O}_4$ @methylcellulose (MC) prepared as a new nano-photocatalyst for degradation of ciprofloxacin from aqueous solution. Environmental Health Engineering and Management Journal 2019; 6(1): 39–41. doi: 10.15171/EHEM.2019.05.

## Article History:

Received: 1 December 2018

Accepted: 12 February 2019

ePublished: 28 February 2019

## \*Correspondence to:

Fatemeh Tamaddon

Email: [ftamaddon@yazd.ac.ir](mailto:ftamaddon@yazd.ac.ir)

## Introduction

Today, the use of drugs, especially antibiotics, is increasing. About 100 000-200 000 tons of antibiotics are produced annually (1). This high level of consumption has led to the entrance of their residues into the environment and caused many problems in this regard (2). The presence of antibiotics in the environment has resulted in drug resistance in humans, as well as an effect on non-target pathogens, the structural alteration of algae in aquatic

resources, and the interference with the photosynthesis of plants (3). The use of antibiotics in human sector, including parts of the services, hospitals, industry, households, as well as the livestock sector, in which antibiotics are used in the form of medicines or supplements for poultry and aquatic animals, is the main source of entrance of these compounds into the environment (4). Although these compounds enter the water or sewage treatment plants through the above-mentioned sources, but due to the



inadequacy of conventional purification technologies, they can return to the environment (5). Studies have shown that most antibiotics are metabolized in the body, and the remaining, about 30-90%, are evacuated into the sewage system without being metabolized (6).

Ciprofloxacin (CIP) is a fluoroquinolones antibiotic, with a broad spectrum bactericidal activity, which is widely used in hospitals to treat bacterial infections. This antibiotic is highly soluble in water and 25% of it is absorbed by the body and the remaining is excreted into the sewage system, in addition, it has sustainability in the environment and contaminates surface and underground water (7). CIP was detected in wastewater and surface water (<1 g/L), hospital wastewater (>150 g/L), and pharmaceutical factory (about 30 mg/L). This antibiotic can be adsorbed in the sludge at a concentration of 42.2 mg/kg (8). In order to remove CIP and other antibiotics, various physical, chemical, and biological methods have been used, including membrane separation (9), ion-exchange resin (10), nanofiltration (11), oxidation (12), and adsorption (13,14). In general, it can be said that most of these methods have not been cost-effective due to the lack of complete degradation of contaminants, as well as low efficiency, high cost of investment and management, and difficult maintenance (15).

Recently, advanced oxidation processes (AOPs), such as ozonation (16), fenton (17), and the use of different photocatalysts (18,19), have been considered and used to reduce the contamination caused by the presence of drug residues and other pollutants in water and environment (20). In the AOPs, radical hydroxyl is produced, which can lead to the oxidation and mineralization of many organic molecules into CO<sub>2</sub> and mineral ions (21). Photocatalytic technology, a green process, has shown great potential for environmental protection. The as-prepared photocatalysts are mainly in the form of powders dispersed in an aqueous solution and are difficult to separate from the treated water after degradation pollutants, which could generate waste and secondary pollution. It is of great importance to design new, very active, and easily recoverable photocatalyst. Thus, the improvement of recyclable kinds of photocatalysts has become the focus of current research. Due to the small size, optical and photocatalytic properties, nanoscale photocatalysts will have a proper efficiency in the degradation of various pollutants. Nanoscale photocatalysts has a larger surface to volume ratio, and are easily dispersed in an aqueous medium, thus, photocatalyst efficiency increases (22). Also, ferrite-based

catalysts with high oxidation and radical hydroxyl (<sup>•</sup>OH) generation in photocatalytic processes can decompose a wide range of organic pollutants (23).

Recently, CuFe<sub>2</sub>O<sub>4</sub> has received attention as a multi-use compound due to its various advantages such as stability, monodispersity, low-cost, high photochemical stability, simplicity, and rapid separation over other catalysts for the pollutants degradation (24-31). Magnetic photocatalytic properties provide a convenient way for separation of the photocatalyst from suspension. CuFe<sub>2</sub>O<sub>4</sub> has mostly been used for photocatalytic degradation of organic effluents in the presence of oxidants, such as hydrogen peroxide (H<sub>2</sub>O<sub>2</sub>). Oxidants are used to accelerate the photocatalytic process, but they are not cost-effective (32,33).

Here, CuFe<sub>2</sub>O<sub>4</sub>@methylcellulose (MC) was prepared via a microwave method as a new magnetic nanobiocomposite photocatalysts. These composites were synthesized for the first time in the water treatment for degradation of CIP without oxidant. In addition, the as-prepared magnetic nanobiocomposite has excellent magnetic properties and could be recycled by magnet and reused for the fourth runs.

### Materials and Methods

FeCl<sub>3</sub>.6H<sub>2</sub>O, CuCl<sub>2</sub>.2H<sub>2</sub>O, NaOH, and MC were purchased from Merck Company. All the chemicals were of analytical grade and used as received without further purification. Deionized water was used throughout the experiment. CIP with a purity of 99% was purchased from Tamad Pharmaceutical Company (Tehran, IRAN). Table 1 shows the structure and properties of CIP used in this study.

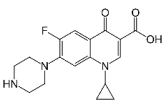
### Preparation of nano-biomagnetic CuFe<sub>2</sub>O<sub>4</sub>@MC

FeCl<sub>3</sub>.6H<sub>2</sub>O and CuCl<sub>2</sub>.2H<sub>2</sub>O with molar ratio of 2:1 were co-dissolved in 50 mL deionized water to get a mixed solution. Afterwards, MC (1 g) was added to the obtained solution under constant stirring and then, sodium hydroxide was added at room temperature under mechanical stirring during an hour. The dark brown solution was subjected to microwave irradiation (3×5 min at 450 W), then, lightweight massive powder formed quickly. The precipitate nano-biomagnetic was washed several times with deionized water and the final product was dried in a vacuum oven at 100°C for 24 hours.

### Analysis and characterization of nano-biomagnetic CuFe<sub>2</sub>O<sub>4</sub>@MC

The microstructure, morphology, and chemical

**Table 1.** Characteristics of ciprofloxacin

Name	Chemical Structure	λ <sub>max</sub> (nm)	Molecular Formula	Class	MW (g/mol)
Ciprofloxacin		276	C <sub>17</sub> H <sub>18</sub> FN <sub>3</sub> O <sub>3</sub>	Antibiotic	331.346

composition of  $\text{CuFe}_2\text{O}_4\text{@MC}$  were investigated by FESEM-EDS (MIRA3TESCAN-XMU). The magnetic properties of  $\text{CuFe}_2\text{O}_4\text{@MC}$  were characterized by VSM (Lake Shore Cryotronics-7404) at room temperature. Thermal stability was evaluated through thermogravimetric analysis (TGA) by STA (PC Luxx 409-NETZSCH) instrument at rate of  $10^\circ\text{C min}^{-1}$  in air. X-ray diffraction (XRD) of the  $\text{CuFe}_2\text{O}_4\text{@MC}$  was recorded in the diffraction angle range of  $2\theta = 15\text{--}70^\circ$  by an X'Pert PRO MPD PANalytical using Ni-FILTERED Cu K $\alpha$  radiation. The concentration of the CIP in solution was measured using a UV spectrophotometer (UV-1800 Shimadzu, Japan) at  $\lambda_{\text{max}} = 276 \text{ nm}$ . The pH of the solution was measured using a pH meter (HANNA, Japan). To generate UV-C radiation, three 6 W Philips lamps (Philips, the Netherlands) were used. The CIP concentration in the real wastewater was measured by an HPLC device (Waters E600, USA) using a column with the properties of  $\text{C}_8$ ;  $259 \times 4.6 \times 5 \text{ mm}$  with UV detector at a wavelength of 272 nm with a hybrid mobile phase HCl 10 micro molar as well as acetonitrile (80:20 v/v), and input flow rate of 1 mL/min. Chemical oxygen demand (COD) was measured by a spectrophotometer (Shimadzu, Japan).

To perform the photocatalytic degradation process, a photoreactor was designed and applied as shown in Figure 1. A plexiglass closed rectangular cube ( $25 \times 10 \times 5 \text{ cm}$ ) was used. The solution volume was 300 mL. Three ultraviolet lamps (UV-C: 6 W) with low pressure were installed at the top of the photoreactor. The height of the lamp above the reactor was 5 cm. The reactor was designed in a way that there was a minimum distance between the catalyst surface and the radiation source to produce more radical hydroxyl by catalytic stimulation. For mixing the solution, a peristaltic pump was used at a flow rate of 1 mL/s.

The photocatalytic activity of  $\text{CuFe}_2\text{O}_4\text{@MC}$  was tested for the degradation of CIP in aqueous solution in a photocatalytic reactor. The suspension of photocatalyst and CIP solution was transferred into a self-designed plexiglass reactor, and stirred in darkness to attain the adsorption equilibrium. Then, the mixture was placed

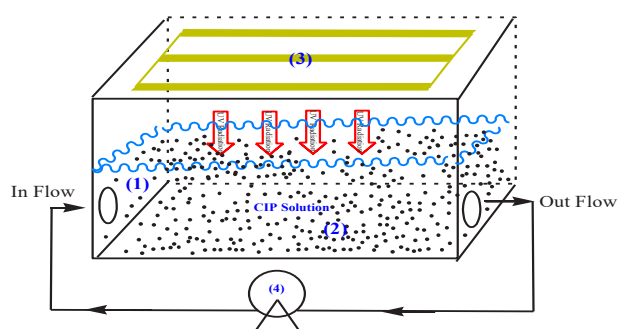


**Figure 1.** The photoreactor used to degrade CIP (1: Plexiglas, 2: photocatalyst dispersed in CIP solution, 3: UV lamps, and 4: peristaltic pump).

inside the photoreactor. Aliquots of the mixture were taken at periodic intervals during the irradiation, and after separation of photocatalyst by a magnet, they were analyzed with the UV-Vis spectrometer. The CIP degradation percentage was calculated as equation (1). CIP degradation (%) =  $100(C_0 - C_t)/C_0$  (1)

where  $C_t$  and  $C_0$  show the attained absorbance value of the CIP solution at different minute periods of time (t) and zero min by a UV-Vis spectrometer, respectively.

HCl and NaOH solutions (0.1 N) were used for adjusting pH. The effects of different concentrations of antibiotics (3, 5, 7, and 9 mg/L), pHs (3, 7, and 11), amounts of photocatalysts (0.025, 0.05, 0.1, 0.2, 0.3, and 0.4 g), and irradiation times (15, 30, 45, 60, 75, and 90 minutes) were investigated in the presence of UV-C lamp on the antibiotic removal efficiency. During the research stages, the investigated parameters were optimized.

## Results

### Characterization of $\text{CuFe}_2\text{O}_4\text{@MC}$

At first,  $\text{CuFe}_2\text{O}_4\text{@MC}$  was prepared by following a new microwave-assisted method. To characterize the given nano-biomagnetic catalyst, various techniques have been employed. Figure 2 shows the FESEM images of  $\text{CuFe}_2\text{O}_4\text{@MC}$ .

To investigate the chemical composition and purity of the as-synthesized magnetic nano-biocomposite  $\text{CuFe}_2\text{O}_4\text{@MC}$ , the energy dispersive spectroscopy (EDS) technique was employed (Figure 3). Figure 4 shows the XRD pattern of the magnetic nano-biocomposite  $\text{CuFe}_2\text{O}_4\text{@MC}$ .

The magnetic properties of the  $\text{CuFe}_2\text{O}_4\text{@MC}$  were evaluated by vibrating sample magnetometer (VSM) at room temperature (Figure 5). The VSM magnetization

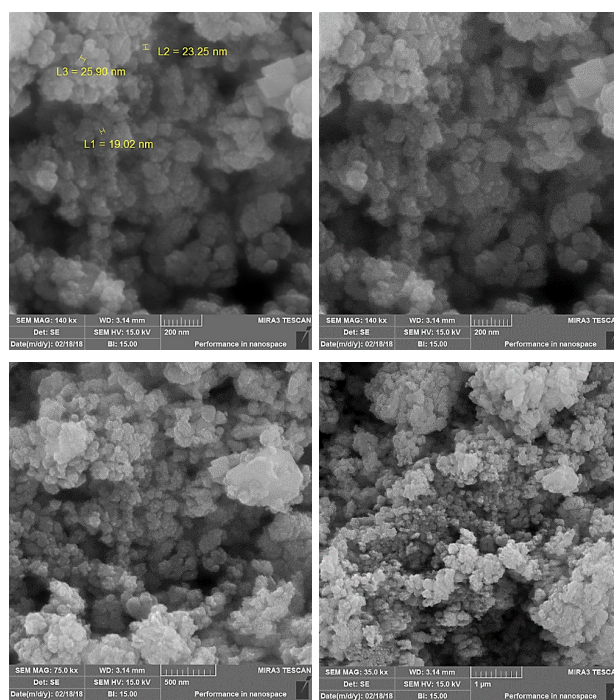


**Figure 2.** FESEM images of nano-biomagnetic  $\text{CuFe}_2\text{O}_4\text{@MC}$  prepared.

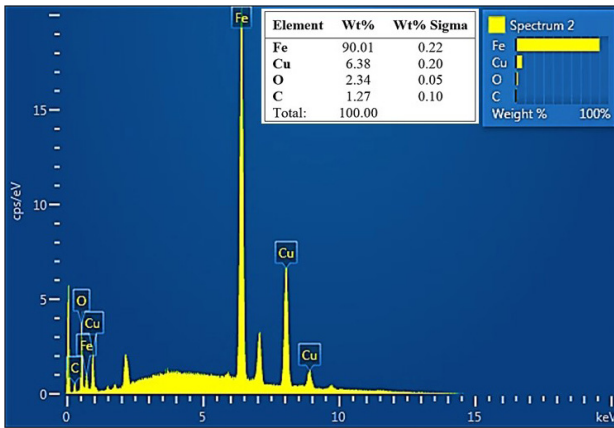


Figure 3. EDS pattern of magnetic nano-biocomposite CuFe<sub>2</sub>O<sub>4</sub>@MC.

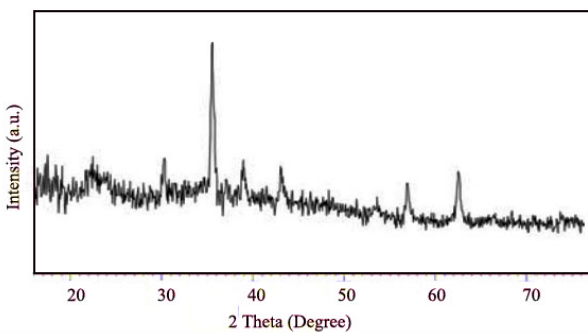


Figure 4. XRD pattern of magnetic nano-biocomposite CuFe<sub>2</sub>O<sub>4</sub>@MC.

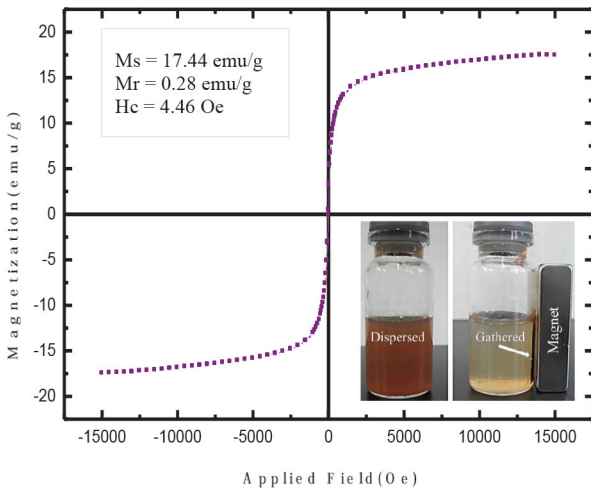


Figure 5. VSM magnetization curve of CuFe<sub>2</sub>O<sub>4</sub>@MC easily separated from the CIP solution under the external magnetic field.

curve of CuFe<sub>2</sub>O<sub>4</sub>@MC proved ferromagnetism. Given that the importance of the thermal stability of photocatalysts at large-scale reactions, the TGA of the CuFe<sub>2</sub>O<sub>4</sub>@MC was performed at temperature of 25 to 800°C at a rate of 10°C min<sup>-1</sup> (Figure 6).

The comparative KBr disc FT-IR spectra of the CuFe<sub>2</sub>O<sub>4</sub>@MC and pure MC at 500-4000 cm<sup>-1</sup> is show in Figure 7.

### Comparison of photolysis, adsorption, and photocatalytic processes in the removal of CIP

The results of the photolysis, adsorption, and photocatalytic process by CuFe<sub>2</sub>O<sub>4</sub>@MC are shown in Figure 8.

### Effect of the initial concentration of CIP

According to Figure 9, the rate of degradation decreased by increasing the initial concentration of antibiotics. The effect of initial concentration of contaminants on the

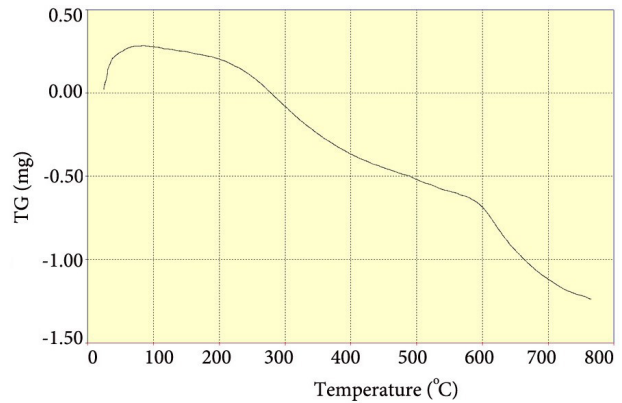


Figure 6. Thermo gravimetric analysis of CuFe<sub>2</sub>O<sub>4</sub>@MC.

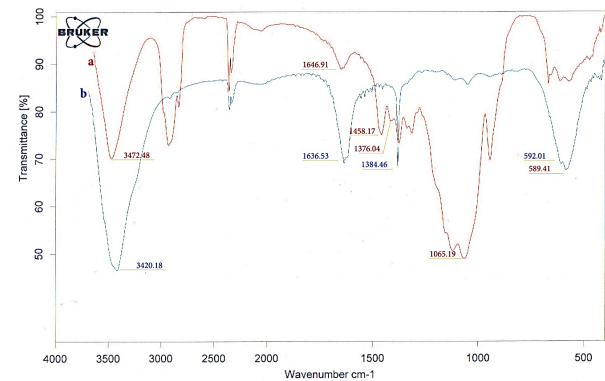


Figure 7. FT-IR of methylcellulose (a) and CuFe<sub>2</sub>O<sub>4</sub>@MC (b).

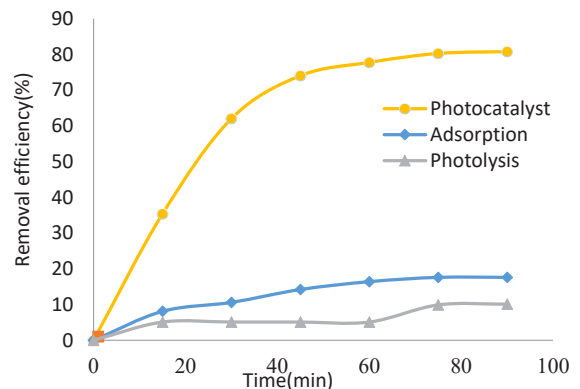


Figure 8. Removal of CIP by various mechanism (contact time = 90 min, pH= 7, CuFe<sub>2</sub>O<sub>4</sub>@MC = 0.2 g, and CIP concentration = 3 mg/L).

performance of photocatalytic process was significant.

### Effect of photocatalyst loading

In photocatalytic processes, the effect of  $\text{CuFe}_2\text{O}_4/\text{MC}$  loading (0.025-0.4 g) on the removal of CIP in laboratory conditions (CIP concentration: 3 mg/L, pH = 7, reaction time: 90 minutes) was investigated. Figure 8 shows the effect of different amounts of photocatalyst on the photocatalytic degradation of CIP (Figure 10).

### Changes of CIP absorption peak intensity vs. irradiation time in the presence of $\text{CuFe}_2\text{O}_4/\text{MC}$

Figure 11 shows the changes of CIP absorption intensity during the photocatalytic process vs. irradiation time. The absorption peak of CIP was  $\lambda_{\text{max}} = 276 \text{ nm}$ .

### Effect of pH on CIP degradation

One of the important factors in photocatalytic processes is pH, which can affect the level of ionization of the material in the solution and the structure of the pollutant molecules by changing the surface charge of the adsorbent. CIP degradation by the photocatalytic process at different pHs is shown in Figure 12.

### Reusability of $\text{CuFe}_2\text{O}_4/\text{MC}$

To examine the stability of photocatalyst, recycling

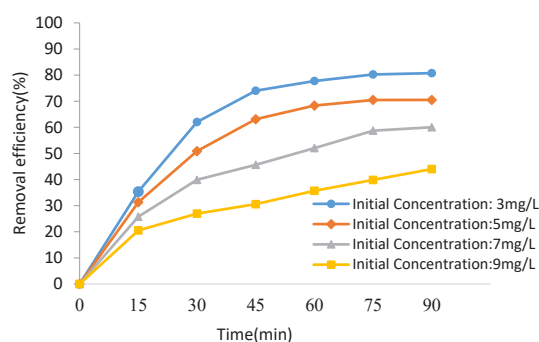


**Figure 9.** Effect of the initial concentration of CIP on the removal efficiency (irradiation time = 90 min, pH = 7, and  $\text{CuFe}_2\text{O}_4/\text{MC} = 0.2 \text{ g}$ ).

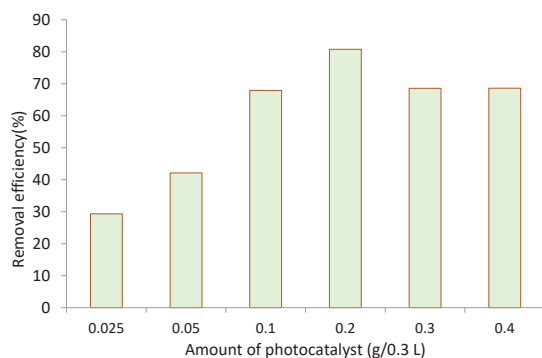


**Figure 10.** Effect of photocatalyst loading on the removal of CIP (pH = 7, CIP concentration: 3 mg/L, irradiation time: 90 min).

experiments were performed and the results are presented in Figure 13.

For each new cycle, photocatalysts were reused for the degradation of a fresh CIP solution under similar conditions after separation of the photocatalyst samples from CIP solution by a magnet. It was easily removed from CIP by washing with deionized water and ethanol, and dried.

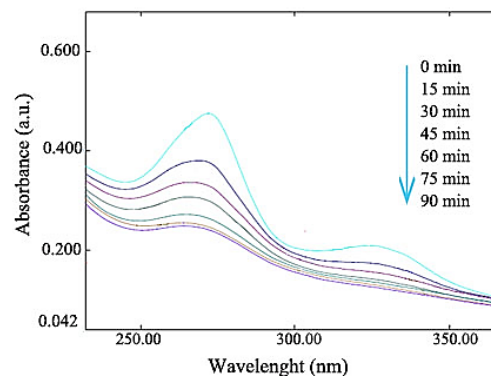


**Figure 11.** The changes in UV-vis spectra of CIP in aqueous solution in the presence of  $\text{CuFe}_2\text{O}_4/\text{MC}$  on different irradiation time (15-90 min).

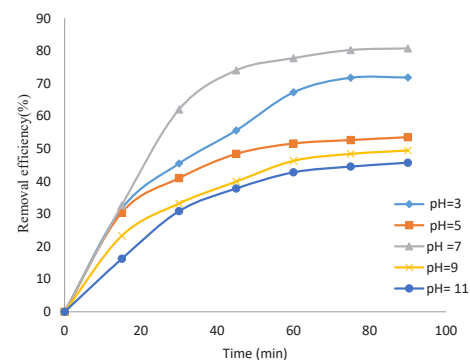


**Figure 12.** Effect of pH on the CIP degradation at different irradiation times (CIP concentration: 3 mg/L and  $\text{CuFe}_2\text{O}_4/\text{MC}$  dosage: 0.2 g).

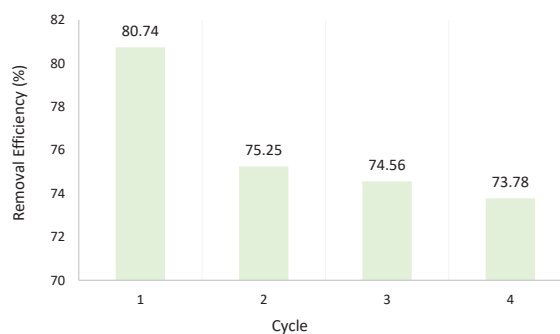


**Figure 13.** Recycle and reuse of photocatalyst for degradation of CIP (CIP concentration: 3 mg/L, photocatalyst dosage: 0.2 g, pH = 7, and irradiation time: 90 min).

### Removal of chemical oxygen demand

In optimal conditions (CuFe<sub>2</sub>O<sub>4</sub>@MC dosage: 0.2 g, CIP concentration: 3 mg/L, pH = 7, and reaction time: 90 minutes), the removal of COD was investigated. The results are shown in Figure 14.

### Examination on real sample

The physicochemical characteristics of wastewater obtained from Kerman University of Medical Sciences, Iran, are reported in Table 2.

By examining the real wastewater sample obtained from the synthetic sample under the optimal conditions, a CIP removal efficiency of 72.87% was obtained. The growth of intervening factors (TSS, COD, etc) causes turbidity in the solution, prevents the penetration of UV radiation, and subsequently, decreases the photocatalytic degradation rate of CIP.

### Discussion

To characterize the given nano-biomagnetic catalyst, various techniques have been employed. Figure 2 shows the FESEM images of CuFe<sub>2</sub>O<sub>4</sub>@MC. The images show the formation of powder consisting of particles with an average size of about 22 nm. As shown in Figure 2, the nano-biomagnetic covers the surface smoothly, uniformly, and compactly, which are loosely aggregated.

EDS spectrum of CuFe<sub>2</sub>O<sub>4</sub>@MC reveals the presence of Cu (6.38% W), Fe (90.01% W), O (2.34% W), and C (1.27% W) as expected amounts for the sample that confirms the chemical structure of this nano-biocomposite (Figure 3). According to the XRD pattern (Figure 4), the peak position and relative intensity of all diffraction peaks for the product matched well with standard powder diffraction data. All the diffraction peaks in the XRD pattern can be indexed to those of the tetragonal structure of copper ferrite (CuFe<sub>2</sub>O<sub>4</sub>) according to JCPDS file No. 34-0425. Room temperature specific magnetization (M) versus applied magnetic field (H) curve measurement of the CuFe<sub>2</sub>O<sub>4</sub>@MC (Figure 5) indicates that the values of coercive force (H<sub>c</sub>), saturation magnetization (M<sub>s</sub>), and remanent magnetization (M<sub>r</sub>) are 4.46 Oe, 17.44 emu/g, and 0.28 emu/g, respectively. All these confirms enough magnetization for simple separation by the external magnetic field. CuFe<sub>2</sub>O<sub>4</sub>@MC uniformly dispersed in CIP solution as shown in Figure 5. After completing the process, CuFe<sub>2</sub>O<sub>4</sub>@MC photocatalyst was easily separated from the CIP solution under the external magnetic field that can be recycled and reused for future runs.

The TGA pattern shows an initial weight loss attributed to water desorption at 100°C, and no further loss of mass is detected up to 600°C, all these confirm the high thermal stability of CuFe<sub>2</sub>O<sub>4</sub>@MC (Figure 6).

The comparative FT-IR spectra of the CuFe<sub>2</sub>O<sub>4</sub>@MC and pure MC show absorption bands of O-H stretching at 3472.48 cm<sup>-1</sup>, C-H stretching at >3000 cm<sup>-1</sup>, adsorbed water stretching at 1646.91 cm<sup>-1</sup>, C-H bending of

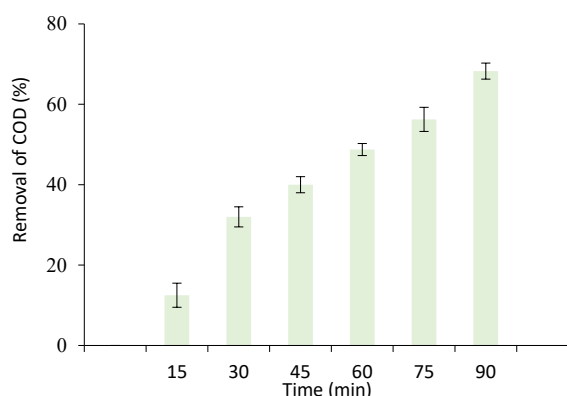


**Figure 14.** Recycle and reuse of photocatalyst for degradation of CIP (CIP concentration: 3 mg/L, photocatalyst dosage: 0.2 g, pH = 7, and irradiation time: 90 min).

**Table 2.** Physicochemical characteristics of wastewater from Kerman University of Medical Sciences

Parameter	Amount
TDS	542 (mg/L)
TSS	18 (mg/L)
BOD <sub>5</sub>	250 (mg/L)
COD	418 (mg/L)
Nitrate	17.2 (mg/L)
Phosphate	18.5 (mg/L)
TKN	76 (mg/L)
Sulfate	358 (mg/L)
pH	7.1
CIP	3 (mg/L)

methylene and methyl groups at 1458.17 cm<sup>-1</sup> and 1376.04 cm<sup>-1</sup>, respectively, and C-O stretching at 1100-1150 cm<sup>-1</sup> for MC (Figure 7a). In the FT-IR spectrum of CuFe<sub>2</sub>O<sub>4</sub>@MC (Figure 7b), the broad peak at 3420.81 cm<sup>-1</sup> was caused by the stretching modes of overlapped OH with aliphatic C-H stretching; the peak at 1636.53 cm<sup>-1</sup> was due to the adsorbed surface water; and the vibration mode of CH<sub>3</sub>-bending was observable at 1384.46 cm<sup>-1</sup>. Two main metal-oxygen bands in the spinel ferrites were located below 1000 cm<sup>-1</sup>. In the synthesized CuFe<sub>2</sub>O<sub>4</sub>@MC, the highest one (ν<sub>1</sub>) was observed at 592.01 cm<sup>-1</sup>. ν<sub>1</sub> is assigned to the intrinsic stretching vibrations of the metal cation at the tetrahedral site M<sub>tetra</sub>-O. The lowest one (ν<sub>2</sub>) was observed at 589.41 cm<sup>-1</sup>, while ν<sub>2</sub> corresponds to the metal cation at the octahedral site M<sub>octa</sub>-O.

Three photolysis, adsorption, and photocatalytic processes have effects on the CIP removal (Figure 8). The removal efficiency in the photolysis process by UV and adsorption by CuFe<sub>2</sub>O<sub>4</sub>@MC was low, which was 10.11% and 17.6% in 90 minutes. The removal efficiency in the 90-minute period was 80.77% in photocatalytic process, it can be concluded that higher removal efficiency of CuFe<sub>2</sub>O<sub>4</sub>@MC for CIP is due to the photocatalytic mechanism versus photolysis and adsorption processes, which is consistent

with the results of the study of Khan et al (34).

The removal efficiency changed from 80.76 to 44.02% by increasing the concentration of CIP from 3 to 9 mg/L during 90 minutes (Figure 9). Increasing the initial concentration leads to a reduction in the UV light penetration into the photocatalyst surface. Photocatalyst excitation and hydroxyl radicals were reduced. Other reasons can be the production of by-products during the process. These by-products compete with the initial concentration of antibiotics in contact with the catalyst, which leads to a decrease in the CIP degradation (35,36). Also, by increasing the initial concentration of antibiotics, more photons are absorbed by CIP and are less involved in photocatalytic process (34), which is consistent with the results of the study of Sayed et al (37).

The results showed that by increasing the amount of photocatalyst up to 0.2 g, the removal efficiency was significantly increased (Figure 10). At higher doses, the removal efficiency ranged from 80.76 to 81.6%, and the dose of 0.2 g was used as an optimal amount for preventing the use of additional photocatalyst. By increasing the dose of photocatalyst, the removal efficiency was raised due to an increase in the active adsorption sites of CIP and radical hydroxyl production (38,39). An increase in the amount of photocatalyst from 0.2 to 0.4 g, due to the turbidity created in the solution, results in a decrease in UV radiation and also a decrease in the radical production of hydroxyl (40). The study of Padmapriya et al confirmed the results of the photocatalyst loading in the present research (41).

Absorption peak intensity declined over time (Figure 11), indicating the rate of CIP degradation by photocatalyst vs. irradiation time. The effect of irradiation time on the CIP removal by increasing the time was due to the production of  $\cdot\text{OH}$  during the process (42), which was more than 80% in 90 minutes.

pH can have a great effect on the removal of organic and inorganic substances from aqueous solutions (43). The rate of CIP removal raised by increasing pH from acidic to neutral pH and declined at pH 11. At pH 7, 80.8% of CIP was removed in 90 minutes (Figure 12). The reason for the high removal efficiency of CIP at pH 7 is that the CIP molecule has a p*K*<sub>a</sub> of 7.8. Due to the protonation of amine groups, the CIP surface appears cationic and positive at pH less than 1.6. Due to the loss of proton from the carboxylic acid group present in the CIP structure, the CIP molecule is converted into anionic form at pH higher than 8.8 (44). As the adsorbent p*H*<sub>pz</sub> is equal to 6.7, the surface charge of photocatalyst is positive and cationic at pH less than p*H*<sub>pz</sub>, and the adsorbent appears as anion with negative charge at pH higher than 6.7. Therefore, at acidic pHs (pH = 3), as the photocatalyst surface and the CIP molecule, both have a positive charge, the electrostatic repulsion is produced and the rate of degradation is reduced (45). The reason for the highest antibiotic stability in the acidic pH is the lack

of the ionized carboxyl group (COOH) (46). As a result, in acidic pH, the solubility of CIP is increased and the removal efficiency is reduced (47). At pH 7, the adsorbent surface charge is negative and CIP has positive surface charge. The electrostatic attraction is then generated and the CIP molecule is transferred to the photocatalyst and causes further degradation of hydroxyl radicals (45). At basic pH (pH = 11), the photocatalyst and CIP molecule both have a negative charge, electrostatic repulsion is generated, and the CIP degradation is reduced (40). Also, due to the high density of negatively charged hydroxide ions, photocatalyst prevents UV radiation and reduces the removal efficiency (43). In alkaline conditions, CO<sub>2</sub> in the solution tends to be converted into HCO<sub>3</sub><sup>-</sup> and CO<sub>3</sub><sup>2-</sup>. These compounds are considered as the degenerative hydroxyl radicals. At high pHs, bicarbonates are converted into carbonate ions, which reduces the oxidation rate by removing OH radicals (48). The study of El-Kemary et al confirmed the results related to pH in the present research (49).

Recycling experiments were performed and the results showed that the photocatalytic activity of the CuFe<sub>2</sub>O<sub>4</sub>@MC had an obvious decrease in the second cycle and subsequently maintained relative stability (Figure 13). The decrease of degradation percentage may be due to the adsorption of intermediate products on the photocatalyst active sites which prohibit the degradation of fresh CIP solution. However, 73.78% of CIP was degraded successfully after the fourth runs, which indicates that the CuFe<sub>2</sub>O<sub>4</sub>@MC could be easily recycled and reused.

The COD removal efficiency of 68.26% was obtained in the optimal conditions during the photocatalytic process. Therefore, the photocatalytic process by CuFe<sub>2</sub>O<sub>4</sub>@MC has a successful role in the removal of carbon groups through conversion of CIP into H<sub>2</sub>O and CO<sub>2</sub>, which is consistent with the results of the study of Malakootian et al (50).

To investigate the kinetics of the photocatalytic degradation of CIP, the pseudo-first order kinetic (Eq. 2) and Langmuir-Hinshelwood kinetic (Eq. 3) models were investigated (43).

$$\ln(C_t/C_0) = -K_{obs}t \quad (2)$$

$$\frac{1}{K_{obs}} = \frac{1}{K_C K_{L-H}} + \frac{C_0}{K_C} \quad (3)$$

Where  $C_0$  is the initial concentration of CIP (mgL<sup>-1</sup>) and  $C_t$  is the concentration of CIP at different times (mgL<sup>-1</sup>).  $K_{obs}$  represents the first-order degradation rate constant (min<sup>-1</sup>),  $K_C$  is the rate constant of the superficial reaction (mg L<sup>-1</sup> min<sup>-1</sup>), and  $K_{L-H}$  represents the adsorption equilibrium constant of L-H model (L mg<sup>-1</sup>).

By plotting  $\ln(C_t/C_0)$  vs. time at different concentrations of CIP, the correlation coefficient was obtained. The results of the pseudo-first order kinetic model investigation are provided in Table 3.

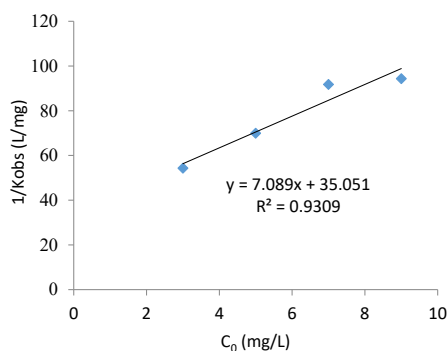
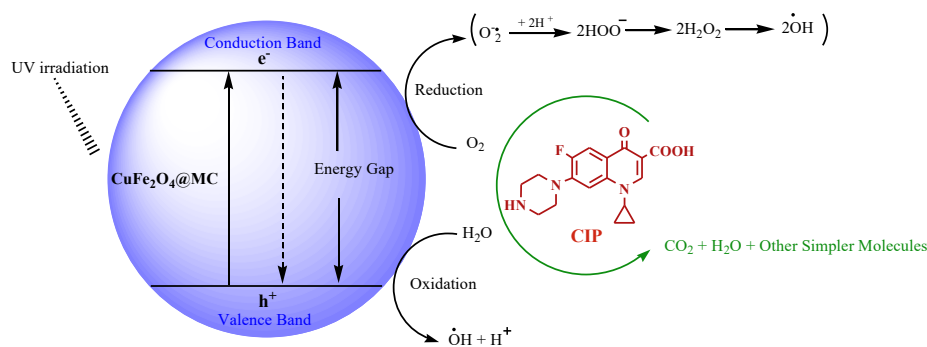
By plotting  $1/K_{obs}$  vs. CIP initial concentration, a straight

**Table 3.** Pseudo-first order kinetic parameters of CIP degradation

$C_0$ (mg/L)	$R^2$	$K_{obs}$ (1/min)	Line Eq.
3	0.902	54.36	$Y = 0.0184x + 0.2251$
5	0.923	69.93	$Y = 0.0143x + 0.1671$
7	0.922	91.74	$Y = 0.0109x + 0.1658$
9	0.929	94.33	$Y = 0.0106x + 0.1463$

line is obtained, through which the equilibrium constant of the L-H model and the superficial reaction rate could be obtained (Figure 15).

The results showed that the photocatalytic degradation process of CIP follows the pseudo-first order kinetic and Langmuir-Hinschwold. Photocatalytic degradation was linearly plotted according to pseudo-first-order degradation kinetic and was consistent with the L-H model. The rate of CIP degradation was related to the initial CIP concentration ( $C_0$ ) and  $K_{obs}$  decreased as  $C_0$  increased. The L-H kinetic model showed good agreement with the initial rates of photodegradation with an appropriate reaction rate constant and substrate adsorption constant values of  $K_c = 0.141$  mg/L min and  $K_{L-H} = 0.202$  L/mg, respectively. An et al investigated the photocatalytic degradation of CIP and reported that degradation follows the pseudo-first order kinetic and Langmuir-Hinschwold kinetics, which is consistent with the results of this study (51). The proposed mechanism for nanoCuFe<sub>2</sub>O<sub>4</sub>@MC-catalyzed photocatalytic removal of CIP contains five

**Figure 15.** Langmuir-Hinschwold kinetic curve.**Figure 16.** The proposed mechanism for photodegradation of CIP by CuFe<sub>2</sub>O<sub>4</sub>@MC.

steps and is shown in Figure 16.

Step 1: Photo-excitation of electron ( $e^-$ )/hole ( $h^+$ ) pair.  
 $\text{nanoCuFe}_2\text{O}_4\text{@MC} + h\nu \rightarrow \text{nanoCuFe}_2\text{O}_4\text{@MC} (e^-_{cb} + h^+_{vb})$

Step 2: Formation of OH $\cdot$  radical.

$\text{nanoCuFe}_2\text{O}_4\text{@MC} (h^+_{vb}) + \text{H}_2\text{O} \rightarrow \text{H}^+ + \text{OH}\cdot$

$\text{nanoCuFe}_2\text{O}_4\text{@MC} (h^+_{vb}) + \text{OH}^- \rightarrow \text{OH}\cdot$

Step 3: Conversion of adsorbed oxygen to superoxide radical.

$\text{nanoCuFe}_2\text{O}_4\text{@MC} (e^-_{cb}) + \text{O}_2 \rightarrow \text{O}_2^{\cdot-}$

Step 4: Neutralization of  $\text{O}_2^{\cdot-}$  to  $\text{HO}_2^{\cdot}$  by protonation.

$\text{O}_2^{\cdot-} + \text{H}^+ \rightarrow \text{HO}_2^{\cdot}$

Step 5: Degradation of CIP by radicals.

$\text{OH}\cdot, \text{HO}_2^{\cdot}, \text{O}_2^{\cdot-} + \text{CIP} \rightarrow \text{CO}_2 + \text{H}_2\text{O} + \text{Other simpler molecules}$

## Conclusion

The CuFe<sub>2</sub>O<sub>4</sub>@MC as a new magnetic nanobiocomposite, was easily synthesized under microwave irradiation in water. This nanobiocomposite, with ferromagnetic and photocatalytic properties, was used to degrade CIP and showed good efficiency. The efficiency of the photocatalytic degradation of CIP by the magnetic nanobiocomposite (CuFe<sub>2</sub>O<sub>4</sub>@MC) was more than adsorption process and UV photolysis. Degradation of CIP increased by increasing reaction time and CIP concentration decreased at neutral pH. Here, the optimal conditions obtained at pH of 7, CIP concentration of 3 mg/L, photocatalyst loading of 0.2 g, and the irradiation time of 90 minutes. The removal efficiency of CIP in the optimal conditions was obtained as 80.74% and 72.87% from the synthetic and real samples, respectively. The removal of COD in the optimal conditions was obtained 68.26% in this process. The photocatalyst was easily recycled and reused after the fourth runs and efficiency reduced about 7% after the fourth runs. The photocatalytic degradation process is an environmentally friendly process. This method can be used to treat large volumes of antibiotic-containing effluent.

## Acknowledgements

The authors gratefully acknowledge Yazd University,



Research Council of Islamic Azad University of Yazd, and Kerman University of Medical Sciences for financial support.

### Ethical issues

The authors hereby certify that all data collected during the study are as stated in this manuscript, and no data from the study has been or will be published elsewhere separately.

### Competing interests

The authors declare that they have no conflict of interests.

### Authors' contributions

All authors contributed equally in the study design, data collection, interpretation, and manuscript approval.

### References

- Bajpai SK, Chand N, Mahendra M. The adsorptive removal of a cationic drug from aqueous solution using poly (methacrylic acid) hydrogels. *Water SA* 2014; 40(1): 49-56. doi: 10.4314/wsa.v40i1.6.
- Gagnon C, Lajeunesse A, Cejka P, Gagne F, Hausler R. Degradation of selected acidic and neutral pharmaceutical products in a primary-treated wastewater by disinfection processes. *Ozone Sci Eng* 2008; 30(5): 387-92. doi: 10.1080/01919510802336731.
- Wei R, Ge F, Huang S, Chen M, Wang R. Occurrence of veterinary antibiotics in animal wastewater and surface water around farms in Jiangsu province, China. *Chemosphere* 2011; 82(10): 1408-14. doi: 10.1016/j.chemosphere.2010.11.067.
- Xu WH, Zhang G, Zou SC, Li XD, Liu YC. Determination of selected antibiotics in the Victoria Harbour and the Pearl River, South China using high-performance liquid chromatography-electrospray ionization tandem mass spectrometry. *Environ Pollut* 2007; 145(3): 672-9. doi: 10.1016/j.envpol.2006.05.038.
- Dirany A, Sires I, Oturan N, Oturan MA. Electrochemical abatement of the antibiotic sulfamethoxazole from water. *Chemosphere* 2010; 81(5): 594-602. doi: 10.1016/j.chemosphere.2010.08.032.
- Kummerer K. Significance of antibiotics in the environment. *J Antimicrob Chemother* 2003; 52(1): 5-7. doi: 10.1093/jac/dkg293.
- Githinji LJ, Musey MK, Ankumah RO. Evaluation of the fate of ciprofloxacin and amoxicillin in domestic wastewater. *Water Air Soil Pollut* 2011; 219(1): 191-201. doi: 10.1007/s11270-010-0697-1.
- Sun SP, Guo HQ, Ke Q, Sun JH, Shi SH, Zhang ML, et al. Degradation of antibiotic ciprofloxacin hydrochloride by photo-Fenton oxidation process. *Environmental Engineering Science* 2009; 26(4): 753-9. doi: 10.1089/ees.2008.0076.
- Calero-Diaz G, Monteoliva-Garcia A, Leyva-Diaz JC, Lopez-Lopez C, Martin-Pascual J, Torres JC, et al. Impact of ciprofloxacin, carbamazepine and ibuprofen on a membrane bioreactor system: Kinetic study and biodegradation capacity. *J Chem Technol Biotechnol* 2017; 92(12): 2944-51. doi: 10.1002/jctb.5316.
- Rajesh AM, Bhatt SA, Brahmabhatt H, Anand PS, Popat KM. Taste masking of ciprofloxacin by ion-exchange resin and sustain release at gastric-intestinal through interpenetrating polymer network. *Asian Journal of Pharmaceutical Sciences* 2015; 10(4): 331-40. doi: 10.1016/j.ajps.2015.01.002.
- Dogan EC. Investigation of ciprofloxacin removal from aqueous solution by nanofiltration process. *Global NEST International Journal* 2016; 18(2): 291-308. doi: 10.30955/gnj.001895.
- Nekouei F, Nekouei S, Noorizadeh H. Enhanced adsorption and catalytic oxidation of ciprofloxacin by an Ag/AgCl@ N-doped activated carbon composite. *J Phys Chem Solids* 2018; 114: 36-44. doi: 10.1016/j.jpss.2017.11.002.
- Sbardella L, Comas J, Fenu A, Rodriguez-Roda I, Weemaes M. Advanced biological activated carbon filter for removing pharmaceutically active compounds from treated wastewater. *Sci Total Environ* 2018; 636: 519-29. doi: 10.1016/j.scitotenv.2018.04.214.
- Peng X, Hu F, Zhang T, Qiu F, Dai H. Amine-functionalized magnetic bamboo-based activated carbon adsorptive removal of ciprofloxacin and norfloxacin: A batch and fixed-bed column study. *Bioresour Technol* 2018; 249: 924-34. doi: 10.1016/j.biortech.2017.10.095.
- Garoma T, Umamaheshwar SK, Mumper A. Removal of sulfadiazine, sulfamethizole, sulfamethoxazole, and sulfathiazole from aqueous solution by ozonation. *Chemosphere* 2010; 79(8): 814-20. doi: 10.1016/j.chemosphere.2010.02.060.
- Tang Y, Ma S, Chen W, Li X, Li L. Catalytic Ozonation of Ciprofloxacin over Cerium Oxide Modified SBA-15 and Toxicity Assessment towards *E. coli*. *J Adv Oxid Technol* 2018; 21(1): 159-69. doi: 10.26802/jaots.2017.0070.
- Salari M, Rakhshandehroo GR, Nikoo MR. Degradation of ciprofloxacin antibiotic by Homogeneous Fenton oxidation: Hybrid AHP-PROMETHEE method, optimization, biodegradability improvement and identification of oxidized by-products. *Chemosphere* 2018; 206: 157-67. doi: 10.1016/j.chemosphere.2018.04.086.
- Ahmad R, Mondal PK. Adsorption and photodegradation of methylene blue by using PANi/TiO<sub>2</sub> nanocomposite. *J Dispers Sci Technol* 2012; 33(3): 380-6. doi: 10.1080/01932691.2011.567172.
- Wang S, Bai J, Liang H, Xu T, Li C, Sun W, et al. Synthesis, characterization, and photocatalytic properties of Ag/TiO<sub>2</sub> composite nanofibers prepared by electrospinning. *J Dispers Sci Technol* 2014; 35(6): 777-82. doi: 10.1080/01932691.2013.813392.
- Klavarioti M, Mantzavinos D, Kassinos D. Removal of residual pharmaceuticals from aqueous systems by advanced oxidation processes. *Environ Int* 2009; 35(2): 402-17. doi: 10.1016/j.envint.2008.07.009.
- Villegas-Guzman P, Oppenheimer-Barrot S, Silva-Agredo J, Torres-Palma RA. Comparative evaluation of photochemical AOPs for ciprofloxacin degradation: elimination in natural waters and analysis of pH effect, primary degradation by-products, and the relationship with the antibiotic activity. *Water Air Soil Pollut* 2017; 228(6): 209. doi: 10.1007/s11270-017-3388-3.
- Khot LR, Sankaran S, Maja JM, Ehsani R, Schuster EW.

- Applications of nanomaterials in agricultural production and crop protection: a review. *Crop Prot* 2012; 35: 64-70. doi: 10.1016/j.cropro.2012.01.007.
23. Casbeer E, Sharma VK, Li X-Z. Synthesis and photocatalytic activity of ferrites under visible light: a review. *Sep Purif Technol* 2012; 87: 1-14. doi: 10.1016/j.seppur.2011.11.034.
  24. Li Z, Lyu J, Sun K, Ge M. Construction of magnetic AgBr/Cu/CuFe<sub>2</sub>O<sub>4</sub> Z-scheme photocatalyst with improved photocatalytic performance. *Mater Lett* 2018; 214: 257-60. doi: 10.1016/j.matlet.2017.12.034.
  25. Hafeez HY, Lakhera SK, Karthik P, Anpo M, Neppolian B. Facile construction of ternary CuFe<sub>2</sub>O<sub>4</sub>-TiO<sub>2</sub> nanocomposite supported reduced graphene oxide (rGO) photocatalysts for the efficient hydrogen production. *Appl Surf Sci* 2018; 449: 772-9. doi: 10.1016/j.apsusc.2018.01.282.
  26. Zhao Y, Lin C, Bi H, Liu Y, Yan Q. Magnetically separable CuFe<sub>2</sub>O<sub>4</sub>/AgBr composite photocatalysts: preparation, characterization, photocatalytic activity and photocatalytic mechanism under visible light. *Appl Surf Sci* 2017; 392: 701-7. doi: 10.1016/j.apsusc.2016.09.099.
  27. Kumar A, Rout L, Achary LS, Mohanty SK, Dash P. A combustion synthesis route for magnetically separable graphene oxide-CuFe<sub>2</sub>O<sub>4</sub>-ZnO nanocomposites with enhanced solar light-mediated photocatalytic activity. *New J Chem* 2017; 41(19): 10568-83. doi: 10.1039/C7NJ02070H.
  28. Karunakaran C, Vinayagamoorthy P, Jayabharathi J. CuFe<sub>2</sub>O<sub>4</sub>-encapsulated ZnO nanoplates: magnetically retrievable biocidal photocatalyst. *J Nanosci Nanotechnol* 2017; 17(7): 4489-97. doi: 10.1166/jnn.2017.14190.
  29. Lu C, Bao Z, Qin C, Dai L, Zhu A. Facile fabrication of heterostructured cubic-CuFe<sub>2</sub>O<sub>4</sub>/ZnO nanofibers (c-CFZs) with enhanced visible-light photocatalytic activity and magnetic separation. *RSC Adv* 2016; 6(111): 110155-63. doi: 10.1039/C6RA23970F.
  30. Karunakaran C, Vinayagamoorthy P, Jayabharathi J. Enhanced photocatalytic activity of magnetically separable bactericidal CuFe<sub>2</sub>O<sub>4</sub>-embedded Ag-deposited ZnO nanosheets. *RSC Adv* 2016; 6(3): 1782-91. doi: 10.1039/C5RA20958G.
  31. Yang H, Yan J, Lu Z, Cheng X, Tang Y. Photocatalytic activity evaluation of tetragonal CuFe<sub>2</sub>O<sub>4</sub> nanoparticles for the H<sub>2</sub> evolution under visible light irradiation. *J Alloys Compd* 2009; 476(1-2): 715-9. doi: 10.1016/j.jallcom.2008.09.104.
  32. Shen JY, Cui ZS, Wu ZW, Wang JX, Ning Q, Lu XM. Simple preparation of CuFe<sub>2</sub>O<sub>4</sub>/C<sub>3</sub>N<sub>4</sub> composites: characterisation and enhanced photocatalysis. *Material Research Innovations* 2015; 19(3): 187-91. doi: 10.1179/1433075X14Y.0000000240.
  33. Le GH, Ngo QT, Nguyen TT, Nguyen QK, Quan TTT, Vu TA. Highly photocatalytic activity of novel CuFe<sub>2</sub>O<sub>4</sub>/GO nano composite in the degradation of phenol from aqueous solution. *Phys Chem* 2017; 7(1): 8-16. doi: 10.5923/j.pc.20170701.02.
  34. Khan MM, Ansari SA, Pradhan D, Ansari MO, Han DH, Lee J, et al. Band gap engineered TiO<sub>2</sub> nanoparticles for visible light induced photoelectrochemical and photocatalytic studies. *J Mater Chem A* 2014; 2(3): 637-44. doi: 10.1039/C3TA14052K.
  35. Hassani A, Khataee A, Karaca S. Photocatalytic degradation of ciprofloxacin by synthesized TiO<sub>2</sub> nanoparticles on montmorillonite: effect of operation parameters and artificial neural network modeling. *J Mol Catal A Chem* 2015; 409: 149-61. doi: 10.1016/j.molcata.2015.08.020.
  36. Chen M, Yao J, Huang Y, Gong H, Chu W. Enhanced photocatalytic degradation of ciprofloxacin over Bi<sub>2</sub>O<sub>3</sub>/(BiO)<sub>2</sub>CO<sub>3</sub> heterojunctions: Efficiency, kinetics, pathways, mechanisms and toxicity evaluation. *Chem Eng J* 2018; 334: 453-61. doi: 10.1016/j.cej.2017.10.064.
  37. Sayed M, Khan JA, Shah LA, Shah NS, Shah F, Khan HM, et al. Solar light responsive poly (vinyl alcohol)-assisted hydrothermal synthesis of immobilized TiO<sub>2</sub>/Ti film with the addition of peroxy monosulfate for photocatalytic degradation of ciprofloxacin in aqueous media: a mechanistic approach. *J Phys Chem C* 2018; 122(1): 406-21. doi: 10.1021/acs.jpcc.7b09169.
  38. Eskandari M, Goudarzi N, Moussavi SG. Application of low-voltage UVC light and synthetic ZnO nanoparticles to photocatalytic degradation of ciprofloxacin in aqueous sample solutions. *Water Environ J* 2018; 32(1): 58-66. doi: 10.1111/wej.12291.
  39. Shetty R, Chavan VB, Kulkarni PS, Kulkarni BD, Kamble SP. Photocatalytic degradation of pharmaceuticals pollutants using N-doped TiO<sub>2</sub> photocatalyst: identification of CFX degradation intermediates. *Indian Chemical Engineer* 2017; 59(3): 177-99. doi: 10.1080/00194506.2016.1150794.
  40. Saien J, Delavari H, Solymani AR. Sono-assisted photocatalytic degradation of styrene-acrylic acid copolymer in aqueous media with nano titania particles and kinetic studies. *J Hazard Mater* 2010; 177(1-3): 1031-8. doi: 10.1016/j.jhazmat.2010.01.024.
  41. Padmapriya G, Manikandan A, Krishnasamy V, Jaganathan SK, Antony SA. Spinel Ni<sub>x</sub>Zn<sub>1-x</sub>Fe<sub>2</sub>O<sub>4</sub> (0.0 ≤ x ≤ 1.0) nano-photocatalysts: Synthesis, characterization and photocatalytic degradation of methylene blue dye. *J Mol Struct* 2016; 1119: 39-47. doi: 10.1016/j.molstruc.2016.04.049.
  42. Amiri Gharaghani M, Malakootian M. Photocatalytic degradation of the antibiotic ciprofloxacin by ZnO nanoparticles immobilized on a glass plate. *Desalin Water Treat* 2017; 89: 304-14. doi: 10.5004/dwt.2017.21378.
  43. Nekouei F, Nekouei S. Comparative study of photocatalytic activities of Zn<sub>5</sub>(OH)<sub>8</sub>Cl<sub>2</sub>.H<sub>2</sub>O and ZnO nanostructures in ciprofloxacin degradation: response surface methodology and kinetic studies. *Sci Total Environ* 2017; 601-602: 508-17. doi: 10.1016/j.scitotenv.2017.05.117.
  44. El-Shafey el SI, Al-Lawati H, Al-Sumri AS. Ciprofloxacin adsorption from aqueous solution onto chemically prepared carbon from date palm leaflets. *J Environ Sci (China)* 2012; 24(9): 1579-86. doi: 10.1016/S1001-0742(11)60949-2.
  45. Iqbal MA, Sharma R, Kamaluddin AR. Surface interaction of ribonucleic acid constituents with spinel ferrite nanoparticles: a prebiotic chemistry experiment. *RSC Adv* 2016; 6(73): 68574-83. doi: 10.1039/C6RA12247G.
  46. Prentice BM, Gilbert JD, Stutzman JR, Forrest WP, McLuckey SA. Gas-phase reactivity of carboxylic acid functional groups with carbodiimides. *J Am Soc Mass Spectrom* 2013; 24(1): 30-7. doi: 10.1007/s13361-012-0506-8.
  47. Chen H, Gao B, Li H. Removal of sulfamethoxazole and ciprofloxacin from aqueous solutions by graphene

- oxide. *J Hazard Mater* 2015; 282: 201-7. doi: 10.1016/j.jhazmat.2014.03.063.
48. DeWitte B, Dewulf J, Demeestere K, Van De Vyvere V, De Wispelaere P, Van Langenhove H. Ozonation of ciprofloxacin in water: HRMS identification of reaction products and pathways. *Environ Sci Technol* 2008; 42(13): 4889-95. doi: 10.1021/es8000689.
49. El-Kemary M, El-Shamy H, El-Mehasseb I. Photocatalytic degradation of ciprofloxacin drug in water using ZnO nanoparticles. *J Lumin* 2010; 130(12): 2327-31. doi: 10.1016/j.jlumin.2010.07.013.
50. Malakootian M, Nasiri A, Amiri Gharghani M. Photocatalytic degradation of ciprofloxacin antibiotic by TiO<sub>2</sub> nanoparticles immobilized on a glass plate. *Chem Eng Commun* 2019; In Press. doi: 10.1080/00986445.2019.1573168.
51. An T, Yang H, Li G, Song W, Cooper WJ, Nie X. Kinetics and mechanism of advanced oxidation processes (AOPs) in degradation of ciprofloxacin in water. *Appl Catal B* 2010; 94(3-4): 288-94. doi: 10.1016/j.apcatb.2009.12.002.